INTERNATIONAL ATOMIC ENERGY AGENCY
UNITED NATIONS EDUCATIONAL, SCIENTIFIC AND CULTURAL ORGANIZATION
INTERNATIONAL CENTRE FOR THEORETICAL PHYSICS
I.C.T.P., P.O. BOX 586, 34100 TRIESTE, ITALY, CABLE: CENTRATOM TRIESTE

H4.SMR/453-6

TRAINING COLLEGE ON PHYSICS AND CHARACTERIZATION OF LASERS AND OPTICAL FIBRES

(5 February - 2 March 1990)

Active-passive Correlation Spectroscopy: A New Technique for Identifying Ocean Color Algorithm Spectral Regions

F. Hoge

NASA Goddard Space Flight Center
Wallops Flight Facility
Wallops Island, Virginia
U.S.A.

Active–passive correlation spectroscopy: a new technique for identifying ocean color algorithm spectral regions

Frank E. Hoge and Robert N. Swift

a reprint from Applied Optics
volume 25 number 15, August 1, 1986

Active–passive correlation spectroscopy: a new technique for identifying ocean color algorithm spectral regions

Frank E. Hoge and Robert N. Swift

A new active–passive airborne data correlation technique has been developed which allows the validation of existing in-water ocean color algorithms and the rapid search, identification, and evaluation of new sensor band locations and algorithm wavelength intervals. Thus far, applied only in conjunction with the spectral curvature algorithm (SCA), the active–passive correlation spectroscopy (APCS) technique shows that (a) the usual 490-nm (center-band) chlorophyll SCA could satisfactorily be placed anywhere within the nominal 460–510-nm interval, and (b) two other spectral regions, 645–660 and 680–695 nm, show considerable promise for chlorophyll pigment measurement. Additionally, the APCS method reveals potentially useful wavelength regions (at 600 and ~670 nm) of very low chlorophyll-in-water spectral curvature into which accessory pigment algorithms for phycoerythrin might be carefully positioned. In combination, the APCS and SCA methods strongly suggest that significant information content resides within the seemingly featureless ocean color spectrum.

I. Introduction

Primary production in the oceans is presently estimated to be about one-third of the total global plant fixation of carbon dioxide.[1] The actual mean and variance of carbon fixation in the sea, however, is highly uncertain. To assist the scientific community in improving the estimates of global productivity, NASA developed the Coastal Zone Color Scanner (CZCS) and launched it aboard the Nimbus-G spacecraft in Oct. 1978. This color sensor was primarily designed to measure or infer the photosynthetic pigments contained in phytoplankton residing within the uppermost water column or near-surface layer of the ocean. Estimates of the attenuation coefficient of downwelling irradiance as well as seston apparently can also be obtained using two-band ratio algorithms.[2] Regarding planktonic pigments in general, only the principal photosynthetic pigment, chlorophyll *a* (plus other chlorophyll-like pigments such as phaeopigment *a*), has been inferred using algorithms applied to ocean color upwelled spectral radiance.

Chlorophyll algorithms for application to remotely sensed upwelled spectral radiance have to date been developed using shipboard truth data. These on-station point measurements are sometimes supplemented by underway fluorometric chlorophyll determinations. The amount and diversity of such truth data are then essentially limited by the speed of the surface vessel. Recently, airborne laser systems have demonstrated that chlorophyll *a* and phycoerythrin fluorescence along with laser-induced water Raman backscatter could be obtained both rapidly and at a high sampling density.[3–6] Accordingly, at laser pulse rates readily available today large numbers of independent measurements may be obtained over wide oceanic regions. Recently, oceanic upwelled spectral radiance measurement capabilities have also been added to an airborne laser spectrofluorometer.[7,8] Voluminous laser-induced and solar-induced spectra synoptically gathered by such an airborne active–passive instrument allow rather high precision studies of the ocean color radiance spectrum via computational algorithms. A typical airborne flight mission produces ~50,000 pair of active–passive observations.

The airborne laser-induced chlorophyll fluorescence from the water column has been shown to yield high correlation to the actual pigment concentration as derived by shipboard extractions and underway fluorescence.[3,9,10] These findings are in spite of known photoplankton fluorescence variability caused by ambient light and nutrient changes.[11] Thus, under the singular assumption that the airborne laser-induced chlorophyll *a* fluorescence is a reliable indicator of the pigment concentration, it will be used as the sole source of truth data for identification and evaluation of the passive ocean color chlorophyll algorithm spectral regions.

In the initial portion of this paper the new active–passive correlation spectroscopy (APCS) technique is introduced and described. The method is then applied to airborne active–passive field data to illustrate its potential for the rapid search, identification, and evaluation of spectral bands or wavelength positions suitable for use in ocean color algorithms for measur-

Frank Hoge is with NASA Goddard Space Flight Center, Wallops Flight Facility, Wallops Island, Virginia 23337; R. N. Swift is with EG&G Washington Analytical Services Center, Pocomoke City, Maryland 21851.

Received 28 January 1986.

Table I. Comparison of Active–Passive and Conventional Correlation Spectroscopy

		A – P CORRELATION SPECTROSCOPY	CONVENTIONAL CORRELATION SPECTROSCOPY
TARGET		Ocean	Atmosphere
SPECIES		Water Column Constituents	Trace Gases
DESIRED QUANTITY	INITIAL	Constituent-Driven Spectral Variability Locations	
	FINAL	Major and Minor Constituent Concentrations	Trace Gas Concentrations
CORRELATION SPECTRUM	FILTER ELEMENT	Actively Measured (Simultaneously)	Mask, Gas, Interferogram
	LOCATION	Digitally Recorded During Experiment	Stored in Instrument
	DYNAMIC	Dynamic	Constant
	CONSTANT		
PHYSICAL MEASUREMENT		Spectral Reflectance (Includes Absorption, Scatter and Emission)	Absorption and Emission

ing chlorophyll. At this time only the three-band or SCA will be evaluated for photoplankton pigment measurement. The APCS technique will also be similarly applied to determine spectral band combinations for the detection and measurement of the accessory pigment, phycoerythrin, since its laser-induced fluorescence is also measurable concurrently with the passive ocean color spectrum. While not specifically addressed herein, it is expected that the APCS technique will in future efforts be extended to standard two-band ratio algorithms, case II waters, other accessory pigments, Gelbstoff, water attenuation, etc. Researchers in other disciplines may also find the technique useful for land and atmospheric spectral pattern recognition.

II. Active–Passive Correlation Spectroscopy

A. Background

Conventional correlation spectroscopy has been used in various configurations for ~60 years.[12] In dispersive, gas filter, and interferometer instruments a known spectrum, gas, or interferogram is stored within the instrument for correlation with the atmospheric trace gas being observed in absorption or emission. Dedicated correlation instruments can possess one or more possible advantages over standard spectrometers including high throughput, spectral simultaneity, data simplicity, and high sensitivity or SNR.

Active–passive correlation spectroscopy described herein differs from these previous applications in several distinct ways. First, it is applied to oceanic waters instead of the atmosphere. Second, the fundamental spectral reflectance, absorption, and emission characteristics of the ocean are not as narrow or well defined as those of the atmosphere. Third, since the spectral character of the ocean is not highly defined, active or laser-induced fluorescence emission spectroscopy is used as known correlation information. A technique will be described for determining the spectral location(s) of the subtle variations in the passive ocean color reflectance caused by water column constituents (phytoplankton pigments, dissolved organic material). In the interest of brevity active–passive correlation and conventional correlation spectroscopy are compared in Table I.

Relative to the APCS technique discussed here, the nearest equivalent remote sensing analog is the oil spill detection method of O'Neil *et al.*[13] They correlated airborne laser-induced fluorescence spectra against similar laboratory fluorescence emission spectra of the target oils overflown. Accordingly, their method could be labeled active airborne–laboratory correlation spectroscopy. Their active-only technique clearly allowed differentiation among a dye, two crude oils, and the general fluorescence background of ocean water.

Another airborne active–passive multispectral scanner (APMSS) instrument (besides the AOL) has been built and successfully flown.[14] Active and passive terrestrial images were obtained. This same APMSS instrument was later used to make active–passive measurements of water depth.[15] No computations of spectral correlation between the two data types were reported for either experiment.

B. Passive Ocean Color Spectrum

In Fig. 1 an idealized solar-stimulated ocean color reflectance spectrum is presented for the case of high and low chlorophyll concentration. It is not distinguished by numerous or prominent spectral features. The most obvious chlorophyll-induced characteristics are (a) the slope change in the nominal 450–570-nm region, (b) the spectral flattening in the 450–510-nm section, and (c) the fluorescence emission in the 675–

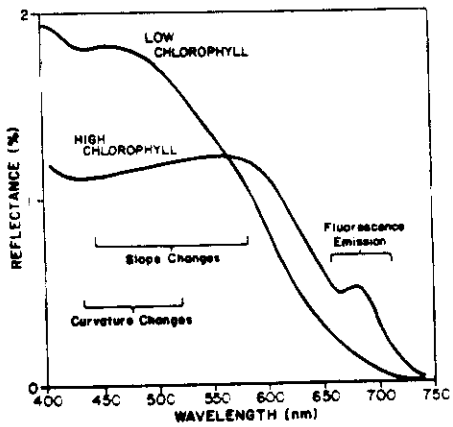

Fig. 1. Idealized low-altitude oceanic spectral reflectance for low- and high-chlorophyll bearing waters. The principal differential chlorophyll features are presently known to be the slope and curvature in the blue/blue-green region and the fluorescence emission in the red.

695-nm segment. For remote sensing of chlorophyll (and phaeopigments) band ratios,[2] curvature,[7,8,16–18] and amplitudes of solar-induced spectral fluorescence emission,[19,20,21] have all been used with varying degrees of success. The band ratio changes have been used most often and form the basis of the satellite CZCS chlorophyll biooptical algorithms.[22] Increasing amounts of chlorophyll pigment also lead to spectral flattening. These curvature variations have recently been used to infer quite accurately chlorophyll from airborne platforms.[7,8,16–18] Only the fundamental intensity (and not slope or curvature) of the fluorescence emission line has to date been used to infer chlorophyll concentration.[8,19,20,21]

C. Active or Laser-Induced Ocean Color Fluorescence Spectrum

Figure 2(a) represents a typical airborne fluorescence spectrum[3,4,6] resulting from laser stimulation at 532 nm. In contrast to passive ocean color spectra, it is distinguished by rather narrow identifiable spectral lines. The laser, phycoerythrin, water Raman, and chlorophyll lines are identified by L, P, R, and C, respectively. This is the type of spectrum against which all correlations herein are performed. The results reported here will be confined only to correlations using the individual spectral lines of the chlorophyll and phycoerythrin pigments. Future plans call for the addition of a shorter wavelength laser transmitter to produce fluorescence from other phytoplankton photopigments.

D. Active–Passive Correlation Spectroscopy Methodology

Figures 2(a) and (b) schematically illustrate paired active and passive measurements as obtained with the Airborne Oceanographic Lidar. For all practical purposes the spectral pair is taken at the same time t_k and essentially within the same footprint. The active data are processed only by normalization with the water

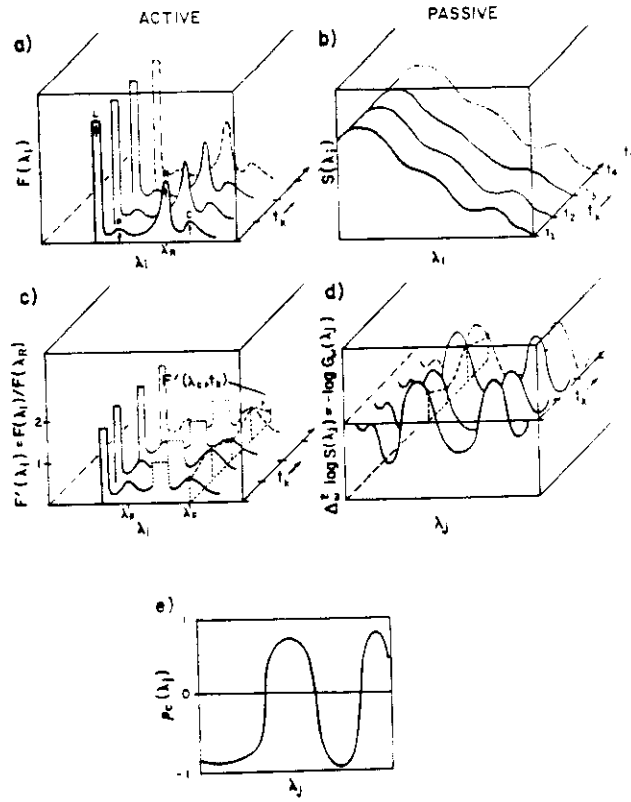

Fig. 2. Schematic illustrations of (a) typical 532-nm laser-induced fluorescence spectrum showing the laser backscatter L, phycoerythrin fluorescence P, water Raman backscatter R, and chlorophyll fluorescence C; (b) idealized solar-stimulated ocean color reflectance spectrum $S(\lambda_i)$; (c) water-Raman-normalized laser-induced fluorescence spectrum $F'(\lambda_i)$; (d) so-called spectral curvature obtained by applying second difference operator to $\log S_i(\lambda)$; (e) representative chlorophyll spectral correlation function $\rho_c(\lambda_j)$ obtained by correlating normalized chlorophyll fluorescence $F'(\lambda_c)$ with $\Delta^2_\lambda \log S(\lambda_j)$ for all λ_j.

Raman backscatter.[4–6,9,23,24] Thus from the original laser-induced fluorescence spectrum, $F(\lambda_i)$, the normalized spectrum $F'(\lambda_i) = F(\lambda_i)/F(\lambda_R)$ is produced as illustrated in Fig. 2(c). The along-track or temporal chlorophyll profile $F'(\lambda_c,t_k)$ is illustrated within Fig. 2(c), and actual profiles of field data will be presented later.

The passive ocean color spectra $S(\lambda_i)$ represented in Fig. 2(b) can be used in an unprocessed form, but unfortunately the high variability of the entire spectral waveform completely masks the desired subtle color variations impressed on the clear ocean water spectrum by the water column constituents. The slope or first derivative spectrum $dS(\lambda_i)/d\lambda$ could likewise be used in the correlation process, but it too contained variability which we were not prepared to correct. (As shall be pointed out later, the field data sets used herein were not specifically gathered for this correlation study but were simply the best available at this time.) The curvature spectrum [related to the second derivative $d_2S(\lambda_i)/d\lambda^2$] does, however, yield results which are reasonably free of unwanted environmental factors.[16–18] Furthermore, it can be applied to uncali-

brated and uncorrected passive ocean color data taken from relatively low aircraft altitudes. All data used here were obtained at 150-m flight altitude. With these considerations in mind we chose to process the passive color data with a curvature algorithm. The algorithm chosen is essentially that of Campbell and Esaias,[18] $\Delta_\omega^2 \log S(\lambda_i)$, where $\Delta_\omega(\ )$ is a difference operator defined by

$$\Delta_\omega f(\lambda) = f\left(\lambda + \frac{\omega}{2}\right) - f\left(\lambda - \frac{\omega}{2}\right). \tag{1}$$

If ω = 30 nm and the operator is applied twice as required, Campbell and Esaias[18] showed that

$$\Delta_\omega^2 \log S(\lambda_i) = -\log G_\omega(\lambda_i), \tag{2}$$

where

$$G_\omega(\lambda_i) = \frac{S_2^2(\lambda_i)}{S(\lambda_i + 30) \cdot S(\lambda_i - 30)}. \tag{3}$$

Thus processing the $S(\lambda_i)$ spectra is performed by starting with data from the bluest spectral band of the instrument, $S(\lambda_i - 30)$, then selecting data from the spectral position 30 nm redder $S(\lambda_i)$ and another 30 nm to the red $S(\lambda_i + 30)$. These three spectral radiances are used to compute $G_\omega(\lambda_i)$ via Eq. (3). Illustrated in Fig. 2(d) is the $-\log G_\omega(\lambda_j)$ or $\Delta_\omega^2 \log S(\lambda_j)$. The index label is changed to j to identify the fact that the original 32 band spectra were first linearly interpolated to "create" additional bands having a width of 1 nm instead of 11.25 nm as actually provided in the passive ocean color subsystem (POCS) of the AOL. The λ_j are successively incremented by 1 nm, and the calculation is repeated until a complete curvature spectrum, such as schematically illustrated in Fig. 2(d), is obtained. For the actual data set to be discussed herein, the procedure is started at 443 nm and conducted 288 times until the final curvature value is obtained from the raw radiances at 701, 731, and 761 nm. The curvature spectrum $G_\omega(\lambda_j)$ is thus shorter than the spectral radiance $S(\lambda_i)$ by 60 nm (30 nm each on the blue and red ends). A curvature spectrum is produced from each raw spectrum $S(\lambda_i)$.

Finally, we wish to produce a correlation spectrum for some desired water column constituent. If the constituent is chlorophyll, scatter plots of $-\log G_\omega(\lambda_j)$ vs $F'(\lambda_c)$ are generated (internal to the computer) for all $1 \le j \le 288$ and for all t_k in a flight line. These scatter plot data then yield a chlorophyll spectral correlation function $\rho_c(\lambda_j)$. This spectral correlation function (SCF) for chlorophyll is illustrated in Fig. 2(e). A spectral correlation function for phycoerythrin $\rho_p(\lambda_j)$ can be similarly calculated by using the normalized laser-induced fluorescence spectrum (evaluated at λ_p) $F'(\lambda_p)$. Typically from 5000 to 10,000 pairs of active and passive waveforms are obtained during the traversal of a flight line. The spectral correlation functions, $\rho_c(\lambda_j)$ and $\rho_p(\lambda_j)$, are usually produced from data acquired along the entire flight line. Both the identification and evaluation of spectral intervals are provided by this spectral correlation function. Values above ±0.8 are selected for further study. The effectiveness of an algorithm is then qualitatively judged by visually comparing along track profiles of the active with the passively derived pigment.

Finer details of the actual handling of active and passive ocean color spectra are provided in Refs. 7 and 8. A brief summary is provided here for the convenience of the reader. Initially, all the passive data were filtered to remove any observations contaminated with sun glint. During the experiment sun glint was minimized by avoiding sampling during the period 1 h on either side of local noon and by pointing the final steering mirror of the AOL ~15° off-nadir and away from the sun. During processing, spectra containing sun glint were recognized by keying on the passive signal in the longest wavelength channel, the center of which was located at ~761 nm. On some of the initial passes (acquired within 1 h of local noon), this filtering procedure amounted to removing as much as 20% of the passive observations, while on some of the later passes as few as 3% of the passive spectra were rejected during processing. The remaining active and passive observations were then subjected to a ten-point simple average. This averaging was done to reduce the volume of data and to minimize any effect on the results from shot-to-shot variability associated with the laser-induced fluorescence measurements. The spatial interval over which the data were averaged amounts to a distance of ~125 m at the ~100-m/s aircraft velocity. Along a typical flight line, some 5000 to 10,000 laser-induced fluorescence waveforms were recorded from which fluorescence emission peaks corresponding to chlorophyll and phycoerythrin can be extracted. An equal number of passive upwelled ocean color radiance spectra were obtained simultaneously. After filtering and averaging, some 500–1000 paired, active and passive, observations remain for analysis.

E. Spectral Curvature Algorithm Forms

In the previous section all linear correlation scatter plots were performed as $-\log G_\omega(\lambda_j)$ vs $F'(\lambda_i)$, where i corresponds to chlorophyll λ_c or phycoerythrin λ_p. Since the laser-induced chlorophyll fluorescence has been shown to be linearly related to the chlorophyll concentration[3,9] C, an algorithm of the form

$$C = A - B \log G_\omega(\lambda_j) \tag{4}$$

is thus inferred. This form has been found to produce more consistent results in our work than the form by Campbell and Esaias,[18]

$$\log C = a - b \log G_\omega(\lambda_m) \tag{5}$$

or the form by Grew and Mayo,[16,17]

$$\log_e C = \alpha - \beta G_\omega(\lambda_m), \tag{6}$$

where λ_m is 490 nm, and A, B, a, b, and α, β are the linear regression coefficients of all the respective forms. Our choice of algorithm in Eq. (4) does not significantly alter the results described since all three forms of the algorithm produce quite good correlation with actual chlorophyll measurements.[7,8,16–18] Of

course, $G_w(\lambda)$ is common to all the algorithms in Eqs. (4), (5), and (6).

Campbell and Esaias[18] found that the curvature algorithm effectively eliminates variations due to changes in incident irradiance while at the same time enhancing spectral features of the water medium. Utilizing a model based on earlier work by Smith and Baker,[25] Campbell and Esaias[18] were able to show that the irradiance reflectance of ocean water exhibits a distinctive curvature spectrum with a large negative curvature at 490 nm. As chlorophyll-like pigments are added to the water this negative curvature monotonically approaches zero. This latter feature is the fundamental physical basis for the high sensitivity of the algorithm to chlorophyll in water.

As indicated previously, the curvature algorithm is essentially a difference operator applied twice to the logarithm of the radiance in the middle spectral band. At least several important consequences result: (1) since this difference is extremely small, relative to the large radiance values involved, the leveraging imposed by the form of the algorithm necessitates high-sensor precision and stability; (2) the calibration of the spectral radiance of the sensor is not a requirement although mission-to-mission stability is essential if the constants in Eq. (4) are to become anchored for real-time use; and (3) the algorithm may be applied in real time to ocean color spectra obtained at relatively low altitudes without serious consequences from atmospherically related effects. (Of course, at high-altitude, additive, independently varying, atmospheric path radiance must be removed before further processing with the three-band algorithm.)

F. Validity of the Airborne APCS Technique

For defining passive ocean color algorithm spectral regions, the validity of the APCS technique rests solely on the validity of the laser data as it relates to actual chlorophyll concentration. If the laser system does not yield fluorescence measurements which are somehow directly relatable to the actual extracted photopigments, the APCS technique will fail.

For the chlorophyll pigment, ship extraction/aircraft fluorescence comparison studies during the past several years indicate that a linear relationship exists between the laser-induced chlorophyll fluorescence signal and corresponding pigment extraction measurements determined onboard cooperating research vessels.[3,9,10] Additionally, in data sets acquired during the shelf edge exchange processes (SEEP) experiment (and utilized for the bulk of the analysis for this paper) corroborating investigators from the University of South Florida and Brookhaven National Laboratory have compared the airborne fluorescence measurements with surface measurements. For all four NASA airborne oceanographic lidar (AOL) SEEP missions the results[26] indicated a linear regression correlation coefficient of 0.93 between the aircraft and ship measurements of chlorophyll in the near-surface layer.

No comparisons have yet been made between airborne phycoerythrin fluorescence and shipboard pigment extractions. Phycoerythrin extraction and measurement methods have been reported.[27,28] However, phycoerythrin measurements are not yet routinely conducted onboard research vessels. Moreover, the lack of a strong cw light source in the ~530-nm region prevents monitoring the phycoerythrin fluorescence signal from a standard flow-through fluorometer.

Inhibition of chlorophyll fluorescence by high-solar irradiance levels[11] could possibly invalidate the laser fluorescence results. Although the effects of solar photoinhibition on airborne laser-induced chlorophyll fluorescence have been reported,[29] we have never seen the effect in our field data. Additionally, lidar receiver linearity must be carefully measured and operating parameters established to avoid misinterpretation of instrument responses as photoinhibition effects. The operational settings of the AOL were established by ground tests and validated further by field experiments.[7,8]

III. Experiment Descriptions

The airborne data utilized to demonstrate the active–passive technique for passive ocean color algorithm band location were acquired primarily during a flight mission conducted in the New York Bight during 1984. Some earlier data gathered during the National Science Foundation's warm core ring (WCR) field experiments in 1982 were additionally used to assess the potential extendibility of the initial results obtained during the SEEP experiments for direct application in other water masses. Results from the above experiments were specifically chosen because (1) simultaneous active and passive ocean color data were available and (2) sufficient contrast between chlorophyll and phycoerythrin patches existed to allow evaluation of the effectiveness of the technique for two different pigments.

The Department of Energy (DOE) sponsored SEEP investigations along the east coast area of the U.S. are designed to assess the assimilative capacity of the Continental Shelf to absorb energy by-products introduced into the near-shore ocean environment from coastal communities and marine activities such as energy production plants and offshore oil operations. This capacity depends to a great extent on rates of removal by sinks in the marine ecosystem. Accordingly, the distribution and abundance of marine phytoplankton over the Shelf and in the adjacent slope water masses are of fundamental importance in this process. The initial SEEP studies, conducted between Feb. and May 1984, are part of a longer range program for the mid-Atlantic region which is planned to continue every 2 years over the next decade. Other institutions participating in these field studies are Brookhaven National Laboratory (BNL), Yale University, LaMont Doherty Geophysical Observatory, University of South Florida, and Woods Hole Oceanographic Institution.

Oceanographic observations within the SEEP test area were acquired from ship (RV Endeavor), moored buoy, satellite, and aircraft platforms. As previously

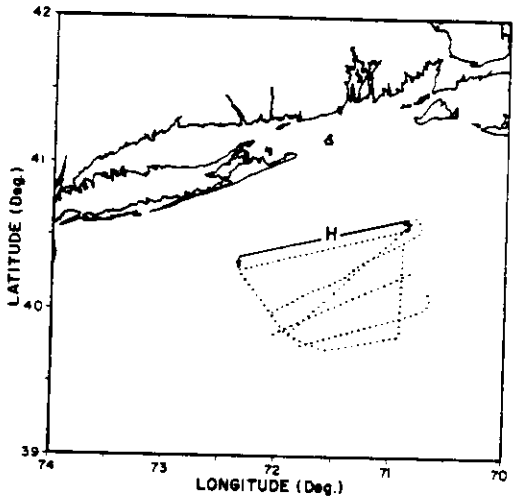

Fig. 3. New York Bight location of the SEEP field test site where most of the airborne active–passive data were obtained. Line *H* had the highest pigment variability and was selected for this study.

mentioned, high correlation has been obtained in comparisons conducted between the laser-induced chlorophyll fluorescence measurements and near-surface chlorophyll data obtained from the research vessel.[26] Similar agreement has been found between airborne surface temperature measurements and surface layer temperature measurements acquired from the research vessel. The airborne ocean surface temperature measurements were obtained with a Barnes PRT-5 IR radiometer and recorded by the lidar data acquisition system. The Eulerean measurements of chlorophyll fluorescence recovered from recording fluorometers attached to the moored buoy lines have yielded interesting results when compared to the nearly synoptic wide-area airborne laser-induced fluorescence values.[26]

Airborne lidar and passive ocean color data were also obtained during the 1982 warm core rings[5,6] experiments. These warm core ring experiments were conducted to provide increased understanding of the biological, physical, and chemical processes associated with warm core rings as they interact with surrounding shelf, slope, and Gulf Stream water masses.

A total of four missions was flown with the Airborne Oceanographic Lidar (AOL)[3–6] and its integral passive ocean color subsystem (POCS)[7,8] during the SEEP experiments. For detailed analysis, we focused our attention primarily on the SEEP mission flown 2 Apr. This mission was chosen because calibrated ocean color data acquired with the NASA Multichannel Ocean Color Sensor (MOCS)[16,17] were also available for comparison and analysis. Active and passive ocean color spectra obtained with the AOL during the 8 Apr. mission were also analyzed to determine general agreement with the 2 Apr. results. However, no corroborative data from the MOCS were available from the latter mission for comparison. In addition, both missions were flown following moderately strong westerly wind events which resulted in a general increase in both the level and spatial variability of chlorophyll *a* concentration within the surface layer, especially in the inner portion of the SEEP study site.[7,8]

The location of flight lines occupied during the 2 Apr. mission is shown in Fig. 3. Only the uppermost line is provided with a letter designation H, which will be referred to during subsequent discussions. (The locations of the 8 Apr. flight lines are virtually identical to those in Fig. 3 and accordingly will not be shown.) The perimeter of the flight lines essentially defines the SEEP study site. The flight lines were designed in conjunction with BNL to complement their sampling strategy with the moored fluorometer arrays. The aircraft data provided periodic synoptic assessment of the distribution of chlorophyll *a* and ocean surface temperature between the buoys, especially alongshelf, which was expected to be the dominant direction of surface current flow and, therefore, the net trajectory for entrained particulate matter.

IV. Application of the Band Location Technique to Airborne Field Data

Line *H* from the 2 Apr. flight was chosen from the SEEP missions for detailed analysis for this paper. This line was primarily selected because the chlorophyll and phycoerythrin concentrations were found to be both elevated and variable. Spatial variability and a degree of noncoherence in the relative concentrations of the two photopigments were considered essential for development and demonstration of the active–passive technique for ocean color algorithm spectral region location development. As will become evident in the succeeding discussion, both chlorophyll and phycoerythrin have considerable effect over wide sections of the passive ocean color spectrum, thus the spatial variability and noncoherence of the photopigments permit any passive chlorophyll or phycoerythrin algorithm to be tested for functionality throughout all regions of a flight line regardless of the relative loading of the other photopigment.

Profiles of laser-induced chlorophyll and phycoerythrin fluorescence are plotted in Fig. 4(a) as a function of distance along the flight line *H*. As mentioned in the previous section, the data in Fig. 4 and in subsequent figures in this section have been subjected to a ten-point simple average. Both photopigments have been normalized with the water Raman backscatter signal to remove effects on the fluorescence signal levels due to variability of attenuation properties in the near-surface layer along the flight track. (A discussion of the normalization technique using the water Raman backscatter signal can be found in Refs. 4, 9, 23, and 24.) A profile of the water Raman backscatter signal is plotted in Fig. 4(b). Profiles of ocean surface temperature, and the passive ocean color signal at 746 nm, are plotted, respectively, in Figs. 4(c) and (d). These latter profiles have been included to provide the reader with a more complete picture of the attendant temperature distribution and relative ambient light levels along the flight line.

The most prominent feature of the laser-induced fluorescence profiles shown in Fig. 4(a) is the large

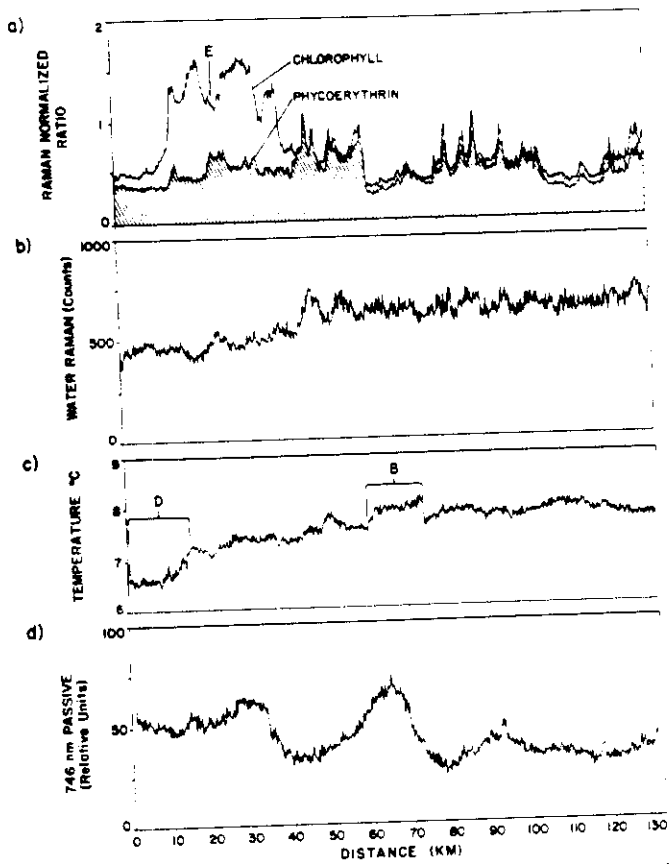

Fig. 4. Along track profiles of line H showing (a) laser-induced chlorophyll a and phycoerythrin fluorescence as normalized by the water Raman backscatter. The low correlation of chlorophyll and phycoerythrin is easily identified in the first 40-km section of the line. (b) Laser-induced water Raman backscatter (note the slight depression in the first 40-km segment of the line). (c) Sea surface temperature along line H. (d) Radiance received in the passive channel centered at 746 nm. The spectral bandwidth is 11.25 nm. (This figure is reproduced from Hoge *et al.*[8])

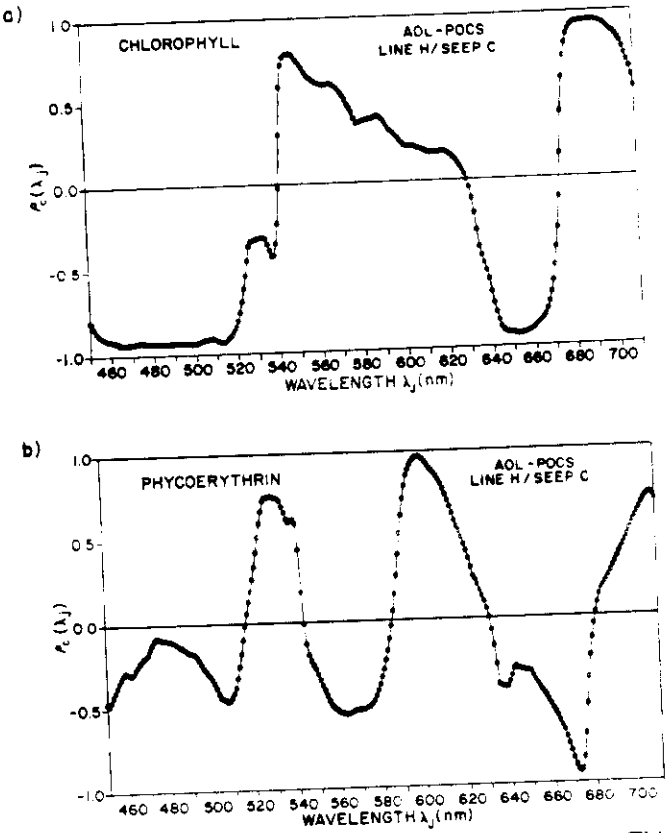

Fig. 5. (a) Chlorophyll spectral correlation function $\rho_c(\lambda_j)$. This function yields spectral regions at 460–510, 645–660, and 680–695 nm where the upwelled spectral radiance variability of the ocean is directly related to chlorophyll pigments. (b) Phycoerythrin spectral correlation $\rho_p(\lambda_j)$. This function gives narrow spectral regions at 600 and ~670 where the upwelled spectral radiance variability is strongly related to phycoerythrin pigment fluorescence. By comparing (a) and (b) it is evident that chlorophyll and phycoerythrin ocean color spectral variability contributions are inversely related at their principal correlation wavelengths and that the ocean color spectrum is essentially invariant to these pigments at 630 nm.

chlorophyll patch located near the eastern end of line H (between 10 and 40 km). Also worth noting are the general coherence between the two photopigment profiles over most of the remaining flight line and the presence of a number of 1–3-km patches of both photopigments. Sufficient detail existed in this flight line (as well as in other flight lines of this SEEP mission) to allow rigorous assessment and evaluation of various combinations of spectral bands for passively determining photopigment concentration.

A. Passive Detection of Chlorophyll and Phycoerythrin

Figure 5 shows the results obtained on flight line H when the curvature values $-\log G_\omega(\lambda_j)$ (computed with the symmetrical; three-band algorithm as described in the preceding section) were linearly regressed for each λ_j against laser-induced chlorophyll [Fig. 5(a)] and phycoerythrin [Fig. 5(b)] fluorescence measurements. In both figures, the linear correlation coefficient ρ_c or ρ_p has been plotted as a function of the wavelength of the center band of the three-band curvature algorithm [Eq. (4)]. Notice that in both figures there are sections of the spectral correlation function where the correlation is high (positive and negative) as well as sections where the computed curvature $-\log G_\omega(\lambda_j)$ is apparently uncorrelated with the photopigment fluorescence $F(\lambda_j)$.

In Fig. 5(a) there is a broad area of high correlation beginning at ~460 nm and extending to ~510 nm. It is thus not surprising that Grew[16,17] and Campbell and Esaias[18] obtained good agreement between spectral curvature measurements and laser-induced chlorophyll fluorescence (and surface truthing chlorophyll measurements) using a three-band algorithm centered at 490 nm. In fact these results suggest that location of the three-band curvature algorithm is not critical in the nominal 460–510-nm region. In this blue segment the observed reduction in curvature and resulting high correlation with chlorophyll fluorescence are probably driven strongly by phytoplankton pigment absorption.

Smaller sections of high correlation are found in Fig. 5(a) in the 645–660- and 680–695-nm regions. Spec-

tral regions where the correlation is strongly negative may be interpreted as a region where the curvature of the spectrum is reduced with increased chlorophyll loading as is the case for the three-band curvature algorithm centered at 490 nm as discussed by Campbell and Esaias.[18] Conversely, strong positive correlation is an indication of increased spectral curvature with higher chlorophyll concentration. The high negative correlation in the 645–660-nm segment is thought to be attributable to absorption by chlorophyll pigments.[30]

The positive correlation seen in the 680–695-nm region may be due in part to observed solar-induced chlorophyll fluorescence. This high correlation is in agreement with other researchers[19–21] who showed that in spite of the lower signals in the red region as much information is present there as in the blue-green region. Increased curvature could also result from additional reflectance in a particular spectral band(s). Moreover, we recognize that strong negative (or positive) curvature in one band will necessarily influence the apparent curvature in adjacent regions as the midpoint of the three-band algorithm progressively approaches the actual spectral feature. Thus, at this point in our investigations, we cannot absolutely determine the physical basis for the apparent curvature variations and resulting high correlations in several of the spectral regions. Finally, the results in Fig. 5(a) suggest that improved chlorophyll measurement might result from combining (or even contrasting) bands from the three high correlation regions. However, for widely separated band segments, the water column sensing depth will probably be different.

In Fig. 5(b) strong positive correlation is found between $-\log G_\omega(\lambda_j)$ and laser-induced phycoerythrin fluorescence when the middle band of the algorithm was centered around 600 nm. At this time a physical basis for this 600-nm peak is difficult to identify since the *in vivo* phycoerythrin fluorescence occurs at 580–585 nm,[31] and its absorption (excitation) maximum is found in the 530-nm region.[27] A second less pronounced area exhibiting high negative correlation can be seen in the band centered near 670 nm. Its physical basis is also puzzling, but like the companion 600-nm peak, it may be due to covariability with other phytoplankton pigments whose functions are coupled to those of phycoerythrin.

Comparison between the two plots of Figs. 5(a) and (b) reveals several other potentially important aspects. First, the correlation with phycoerythrin fluorescence diminishes to low values in the 460–510-nm spectral region where there is high correlation with chlorophyll fluorescence. Low correlation ($\rho_p < 0.5$) with phycoerythrin fluorescence is also found in the 645–660- and 680–695-nm regions where the correlation with chlorophyll fluorescence is also high. Conversely, in the spectral region near 600 nm, where the correlation with phycoerythrin fluorescence is strongest, there is a broad spectral region where the correlation with chlorophyll fluorescence is at a minimum. Second, and perhaps more important to the sensor band and algorithm selection process, the plots of the spectral correlation functions in Fig. 5 provide a clear indication of the profound influence of both photopigments at several specific but often widely separated spectral regions. This aspect is an especially critical consideration for satellite-borne passive ocean color sensors where a spectral band suitable for removing atmospheric effects must be selected and where budget and logistical constraints limit the number of available channels. Current techniques for processing CZCS imagery utilize the spectral channel centered at 670 nm to correct atmospheric effects on the bluer channels involved in the in-water algorithm for determining chlorophyll concentration. Third, the 630-nm region of the ocean color spectrum appears to be relatively invariant to both chlorophyll and phycoerythrin pigments since the spectral correlation functions have very low values there. These type regions may thus be useful for atmospheric correction.

The presence of three high-correlation peaks also strongly suggests that significant information content resides within the ocean color spectrum and that useful information can be found outside the most obvious slope, curvature, and fluorescence emission regions of chlorophyll (refer again to Fig. 1). While these specific findings are new, this general information-content finding is in agreement with Lin *et al.*[19] They found chlorophyll information within numerous regions of the ocean color spectrum using eigenvector analysis of airborne data together with ship truth. The APCS technique appears to be easier to utilize than eigenvector techniques. Furthermore, the correlation method vividly shows the participating spectral bands without hand-selecting the study spectral regions. Finally, the algorithm can be specifically applied to bands of interest and thus is not limited to eigenvectors whose physical meaning is somewhat obscure.

Computed $-\log G_\omega(690)$ and $-\log G_\omega(600)$ values from the three-band algorithm, which were found from Fig. 5 to have the highest correlation with chlorophyll and phycoerythrin, were next plotted in profile form in Fig. 6. These plots allow visual assessment of the detailed characteristics of the $-\log G_\omega(\lambda_j)$ values by direct comparison with the respective photopigment fluorescence signals. The estimated chlorophyll concentration computed from the curvature algorithm with the middle band centered at 690 nm is plotted in Fig. 6(a) as a function of distance along flight line H together with laser-induced chlorophyll fluorescence originally shown in Fig. 4(a). For convenience of handling and plotting, both the active and passive concentration estimates have been autoscaled. As expected from the high-correlation coefficient found in Fig. 5(a), the two profiles show good agreement over the entire flight line even down to relatively small scale features. Similarly, a profile of $-\log G_\omega(600)$ is plotted in Fig. 6(b) together with phycoerythrin fluorescence [originally shown in Fig. 4(a)]. Again good agreement is apparent over the entire flight line. Note particularly how well the phycoerythrin algorithm performs in the high-chlorophyll region (10–40 km).

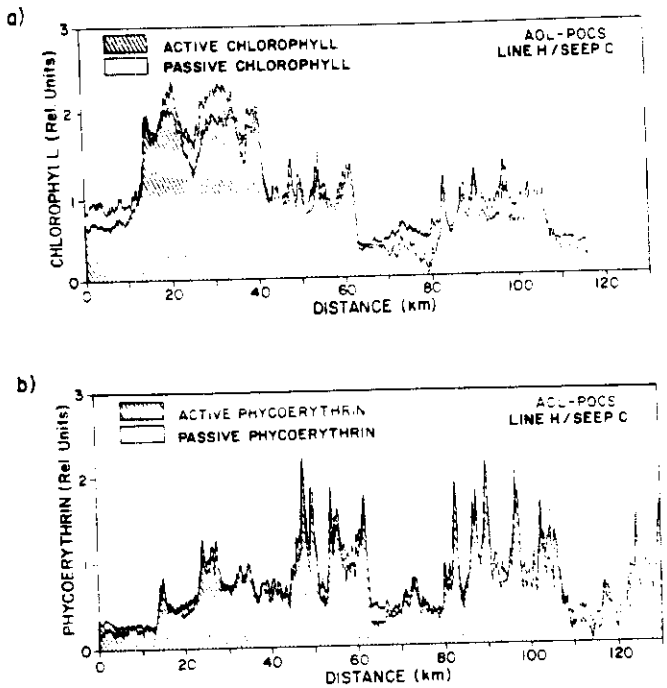

Fig. 6. Passively derived (a) chlorophyll at 690 nm and (b) phycoerythrin at 600 nm using a curvature algorithm of the form given in Eq. (4). The water Raman normalized laser-induced chlorophyll and phycoerythrin fluorescence are, respectively, plotted in each section for comparison purposes. The data were obtained along line *H* (Fig. 3) using the active and passive capabilities of the airborne oceanographic lidar.

This initial application of our technique to select passive spectral bands utilizing data acquired with the AOL operated in a dual active–passive mode was very encouraging. In short, these results showed that

(1) several regions of high correlation were determined for chlorophyll measurement;

(2) one region was identified which showed particularly strong correlation with phycoerythrin fluorescence;

(3) spectral areas of high correlation in the chlorophyll regression plot correspond to the lower bands of correlation in the phycoerythrin regression plot and vice versa; and

(4) a spectral segment which is relatively invariant to both chlorophyll and phycoerythrin pigments was observed.

Although agreement between the results from the band selection algorithm and the photopigment fluorescence measurements appears to provide considerable evidence of the potential utility of the technique for passive ocean color band selection, verification of the curvature results with a second independent passive sensor would assure that there was no instrument related artifacts associated with the results. We, therefore, undertook examination of some data sets containing concurrent passive ocean color measurements acquired with the NASA MOCS during the SEEP experiment and WCR studies (prior to implementation of the passive ocean color subsystem into the AOL).

Spectra collected with the MOCS were processed through the band selection algorithm using essentially the same procedure described for the AOL passive spectra. The resulting $-\log G_\infty(\lambda_j)$ values were then regressed independently against the AOL active laser-induced photopigment fluorescence measurements. The resulting spectral correlation function plots (not shown) produced quite similar results, although the peak correlation coefficients were slightly lower, especially for phycoerythrin estimation. Slightly lower peak regression coefficients would be expected since the MOCS passive and AOL active observations were not obtained from the same exact footprints and because of the differences in methods of real-time data capture and handling between the two sensors. For example, in its present configuration, the MOCS is essentially locked in a nadir viewing position and thus cannot be pointed away from the solar glint pattern. Moreover, the MOCS integrates approximately fifteen ocean color spectra per second from near-nadir pixels. Accordingly, individual observations containing sun glint could not be effectively filtered from surrounding observations which are glint-free.

Profiles of estimated chlorophyll and phycoerythrin concentration developed from MOCS ocean color spectra using the three-band curvature algorithm are plotted in Fig. 7. Respective estimates of each of the photopigments computed from the AOL passive data are included for comparison purposes. The computed $-\log G_\infty(490)$ values were selected for plotting the profiles of estimated chlorophyll in Fig. 7(a) rather than the $-\log G_\infty(690)$ values previously shown in Fig. 6(a). This change in band selection was necessary because spectral coverage of the MOCS extends only to ~700 nm, thus precluding accurate computation of a $-\log G(\lambda_j)$ value at 695 nm. Moreover, the MOCS signal levels were too low in the red spectral region to yield satisfactory comparative results even at 660 nm. Other potentially useful passes were flown earlier in the mission in conditions of higher solar illumination. The presence of sun glint during these earlier passes (>20% on initial flight lines compared with 3% on the final line *H*) probably accounts for much of the degradation in the overall agreement between the two sensors.

Profiles of estimated phycoerythrin concentration are shown plotted in Fig. 7(b) using $-\log G_\infty(\lambda_j)$ values located at 595 and 600 nm for the MOCS and AOL/POCS, respectively. Although general agreement between the two phycoerythrin concentration profiles in Fig. 7(b) is reasonable over much of the flight line, the level of agreement is certainly below that found for the chlorophyll profiles in Fig. 7(a). This is especially the case in the initial 45 km of the flight line where considerable influence from chlorophyll appears to be exhibited in the MOCS phycoerythrin profile when it is compared with chlorophyll profiles shown in Figs. 6(a) or 7(a). Note particularly that the features located between 15 and 35 km along the flight line in Fig. 7(b) appear to be noncoherent. The reason for the lower agreement of the passive MOCS phycoerythrin profile

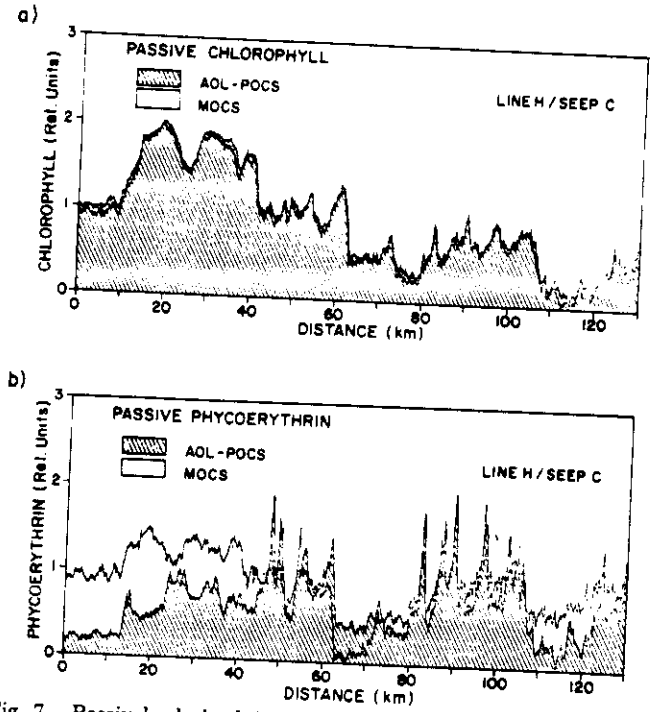

Fig. 7. Passively derived (a) chlorophyll and (b) phycoerythrin using an algorithm of the form in Eq. (4). The data were obtained with the MOCS and the AOL–POCS. The chlorophyll profile was generated using a curvature algorithm centered at 490 nm for both sensors. The phycoerythrin profile was obtained from curvature algorithms centered at 595 nm (MOCS) and 600 nm (AOL–POCS).

is unknown at this time. It may be due in part to differences in the spectral bandwidth of the sensor channels or to the lower sensitivity of the MOCS in the redder spectral region. The bandwidth of the MOCS channels is ~15 nm, while the AOL spectrometer channels are 11.25 nm in width. The influence of chlorophyll in the MOCS spectra in the vicinity of 600 nm and the differing channel bandwidth may also attribute to the slight difference in the wavelengths where $-\log G_w(\lambda_j)$ values from the two sensors were found to have the highest correlation with laser-induced phycoerythrin fluorescence.

The potential utility of the technique for locating passive ocean color bands appears successful and worthy of continued development. The actual chlorophyll and phycoerythrin results (i.e., the algorithm and bands themselves), however, require further study. The potential of these findings would be considerable if the results were found to be reasonably universal, i.e., if similar results are obtained at other oceanic locations and under differing environmental conditions. This is especially the case for the passive phycoerythrin algorithm since no alternative passive method for estimating this pigment has been previously published. To validate the technique further and to potentially establish more of a basis for universality for the particular bands thus far identified for determining photopigment concentration, flight lines *A* and *G* (not shown) from the same SEEP mission were also examined in the same way. Qualitatively, the results were found to be essentially the same. The spectral regions found to produce the highest correlation with the respective photopigments were consistent with the findings for flight line *H*. Quantitatively, however, the values of the highest correlation coefficients were found to be somewhat lower. The remaining three missions flown in connection with the SEEP experiments were not as suitable for performing this type of analysis. During the first two missions which were flown in early March, the concentration levels and spatial variability of chlorophyll and phycoerythrin were considerably lower, thus yielding less consistent results when processed with a linear regression program. The 8 Apr. mission was flown under overcast conditions where sky contributions to the passive ocean color signal are higher. Nonetheless, the flight lines from the 8 Apr. mission did show results which were in good general agreement with those from 2 Apr. However, the peak correlation coefficient values were somewhat lower.

Finally, we evaluated a data set from the 1982 WCR experiment which contained both active and passive ocean color data. Since the WCR experiments predated the relatively recent addition of the passive subsystem to the AOL, we utilized passive ocean color observations which were acquired with the MOCS for direct comparison with simultaneous AOL laser-induced photopigment fluorescence measurements. The WCR data set was regarded as particularly valuable since it contained observations from several new water masses including the Atlantic outer shelf, slope, Gulf Stream, and Sargasso Sea water types and since it was acquired nearly 2 months later in the year. Thus there existed a reasonable potential for the presence of entirely different suites of phytoplankton.

The flight lines of the 24 June WCR mission were arranged to cross the ring at various angles with each line passing through the ring center. The general levels of photopigment concentration were relatively low. Moreover, the highest levels of chlorophyll (1.5 μg/liter maximum) were found near the center of the ring while pockets of higher phycoerythrin concentration were found in the ring boundary region, both north and south of the ring. There was little spatial variability of phycoerythrin levels in the east–west direction. As a result, only flight line 6 (flown from north to south) was found to contain sufficient contrast between the two photopigments to allow evaluation of the bands identified and selected using subsequent SEEP data.

Figure 8(a) shows a comparison between laser-induced chlorophyll fluorescence and passive (MOCS) chlorophyll values as a function of distance along the flight line. Similarly, Fig. 8(b) shows a comparison between laser-induced phycoerythrin fluorescence and estimates of the relative level of the phycoerythrin concentration using passive ocean color spectra from the MOCS. The passive ocean color spectra from the MOCS were processed through the same three-band algorithms previously described for the data presented in Fig. 7. The ~10-km gap appearing in both the

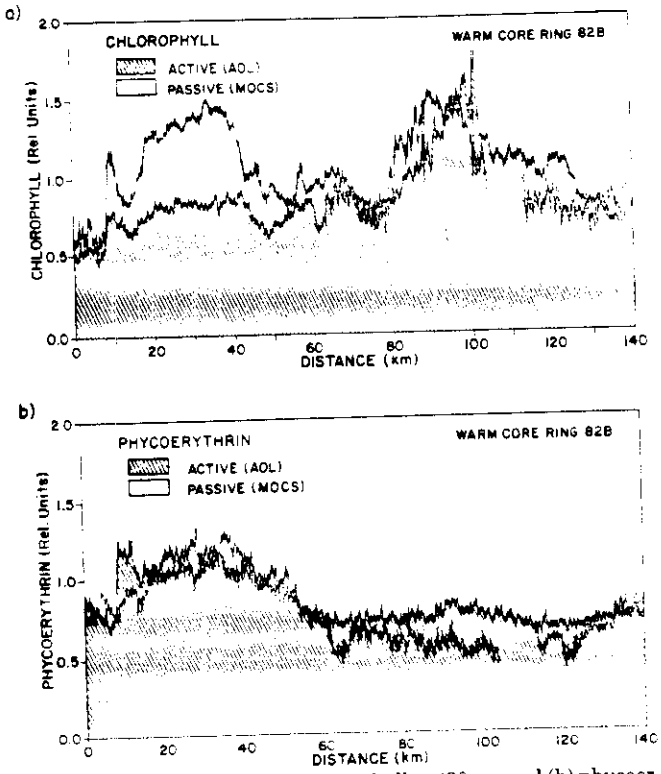

Fig. 8. Passively derived (a) chlorophyll at 490 nm and (b) phycoerythrin at 600 nm using an algorithm of the form in Eq. (4). The data were obtained with the MOCS during a warm core ring mission in 1982. The AOL water–Raman normalized laser-induced chlorophyll and phycoerythrin fluorescence are, respectively, plotted (shaded) in each section for comparison purposes.

MOCS chlorophyll and phycoerythrin profiles beginning near the 105-km point in the flight line resulted when the data from the previous portion of the flight line were dumped from memory to tape.

The agreement between the profiles of chlorophyll concentration in Fig. 8(a) is in much lower agreement than seen in the results from the later SEEP missions or from results presented previously by Grew[16,17] and Campbell and Esaias.[18] Although both profiles appear to exhibit similar trends over much of the flight line, an apparent scale difference exists between the 0–80-km section and the remaining portion of the flight line. In addition, there is a considerable offset between the peak area of the observed chlorophyll patch seen between 80 and 105 km. By contrast, the general level of coherence between the laser-induced phycoerythrin fluorescence profile and the phycoerythrin concentration profile estimated from the MOCS ocean color data appears to be in quite reasonable agreement over much of the flight line. It is also very evident that the large patch of chlorophyll located between 80 and 105 km [Fig. 8(a)] does not appear to influence the MOCS phycoerythrin profile which remains essentially parallel to the laser-induced phycoerythrin profile in that area of the flight line.

V. Summary, Discussion, and Conclusions

We have described in detail a new active–passive correlation spectroscopy technique which allows regions of ocean color spectral reflectance variability to be directly related to the presence of specific fluorescent waterborne constituents. Subtle variations in the solar-induced ocean color reflectance spectrum are shown to be vividly revealed by correlating spectral curvature changes with laser-induced fluorescence of chlorophyll and/or phycoerythrin. The three-band curvature correlations against chlorophyll fluorescence are sequentially executed in 1-nm intervals across the ocean color spectrum to generate a so-called spectral correlation function. Correlation values exceeding ±0.8 then signify important spectral regions of ocean color covariability with the known fluorescent constituent(s). In turn, the identified color spectral segments are regarded as the most optimum available for placement of passive sensor bands and resulting application of their computational algorithms. It has also been shown that the described method differs considerably from conventional correlation spectroscopy in that the known correlation data (laser) are actually obtained simultaneously with the airborne passive ocean color spectra. While only applied herein to ocean color spectra, the technique is also expected to have important application to remotely sensed land and/or atmospheric radiances.

The recent addition of a passive ocean color subsystem into the AOL has allowed the acquisition of active and passive ocean color measurements from essentially the same footprint. The relative mobility afforded by the aircraft platform, coupled with the 6.25-pps laser transmitter, provides a relatively high sampling density of paired observations over wide areas and differing water types. This capability has in turn facilitated development of a technique for identification and verification of algorithm spectral regions for remotely determining chlorophyll concentration. This technique may also be applicable for the development of algorithms for passively measuring other phytoplankton photopigments as well as other waterborne constituents that can be sensed with an active lidar system.

The approach has been to select initially a form for the algorithm. A number of forms are possible, and in this initial investigation we selected a three-band curvature algorithm with sidebands that are separated from the center band wavelength by 30 nm. Although this choice was in part arbitrary, it was based on previous success demonstrated by an algorithm of this type. This three-band algorithm is convoluted with (or applied stepwise in 1-nm intervals to) the upwelled radiance spectrum. The logarithm of the resulting spectral curvature values are then linearly regressed against the water-Raman-normalized laser-induced chlorophyll (or phycoerythrin) fluorescence measurements obtained concurrently during the flight mission. The spectral correlation functions thus generated are then examined to reveal spectral regions where acceptable correlation between the $-\log G_a(\lambda_i)$ values and the

laser-induced fluorescence values has been achieved. Useful spectral regions more narrow than ~15 nm were not expected since the AOL–POCS instrument bandwidth is only 11.25 nm. Finally, the $-\log G_\omega(\lambda_j)$ values showing the highest correlation are graphed in a profile form along with the fluorescence measurements to allow more detailed visual examination and to reveal additional characteristics of the resulting passive constitutent estimation.

The initial application of the technique to data obtained in the New York Bight during the 1984 SEEP experiment was extremely successful. In particular, the processed passive ocean color data obtained on flight line *H* (2 Apr. 1984), which exhibited relatively high chlorophyll concentration variability (0.5–6.0 μg/liter) and areas of noncoherence between chlorophyll and phycoerythrin fluorescence levels, resulted in regression coefficients >0.95 and revealed few areas of inconsistency with the concurrent chlorophyll and phycoerythrin laser-induced fluorescence measurements. These results were essentially verified or validated by processing spectra obtained by an independent passive ocean color instrument (MOCS) also flown simultaneously onboard the NASA P-3A aircraft.

Attempts to apply the same techniques on other flight lines flown during the same mission were also successful, although somewhat lower correlation values were obtained, potentially due to the greater amounts of sun glint observed on these other passes. Similar results were obtained when the technique was applied to data sets obtained during a subsequent flight which occupied the same flight lines ~1 week later. In an attempt to ascertain the potential universality of the spectral bands identified during the SEEP experiment, passive ocean color data obtained with the MOCS on a mission flown 2 years earlier in connection with the WCR studies were also processed through the three-band curvature algorithm. The resulting profiles of estimated chlorophyll and phycoerythrin were shown to be in reasonable agreement with respective laser-induced fluorescence measurements of those constituents.

Although the correlation between the $-\log G_\omega(\lambda_j)$ values computed from the passive data (using the spectral bands determined to be most optimal) produced results which varied from highly correlated to more moderate levels of correlation, the band location technique itself appears to have been satisfactorily demonstrated. Both the placement of sidebands in the three-band curvature algorithm relative to the center band and the form of the algorithm itself were not optimized during correlation processing. Numerous separations of the sidebands are possible, and the 30-nm symmetric sideband arrangement may not yield the most optimum results. Moreover, other forms need to be examined. These include in-water two-band ratio algorithms such as those currently utilized in processing CZCS imagery.

Various environmental factors may have influenced the results. Cloud cover and ambient light levels were not routinely monitored on the initial missions flown with the AOL passive ocean color subsystem. Recent modifications to the AOL will ensure that these parameters will be continuously monitored. Questions need to be resolved regarding the effects on these results of other water types, high sediment, and/or dissolved organic material loading (Gelbstoff), and changes in phytoplankton assemblages. For example, different phytoplankton species could contain a considerably different ratio of photopigments than were encountered along line *H*, and this in turn could affect the spectral location of the bands and degree of correlation achievable with the form of a particular algorithm.

We are, however, somewhat limited in the extent to which these issues could be addressed with available data sets. The instrument had only been configured to operate in the dual active–passive ocean color mode since spring 1984, restricting the investigations to a relatively few data sets. In general, the AOL has been flown in support of large-scale oceanographic experiments that have multi-institutional participation. In these experiments, the flight patterns as well as the activities onboard the research vessel are generally designed to provide data required by the participating oceanographers, and information essential to improving remote sensors is often obtained more incidentally than by design. Accordingly, information on speciation, auxiliary photopigments (other than chlorophyll *a*), phaeophytin, dissolved organic material concentration, and the attenuation properties of the near surface ocean layer, all of which would be useful in analyzing results, are essentially unavailable in our existing data sets.

Nonetheless, the results thus far obtained using the passive ocean color band selection technique indicate that photopigments contained in chlorophyll exert profound influences in specific regions of the entire ocean color spectrum. These areas extend well into the red region beyond 670 nm. Currently the 670-nm CZCS band is assumed to be free of contributions from within the water column and thus is being utilized to correct CZCS imagery for atmospheric effects.

The results herein also suggest the presence of windows within the ocean color spectrum where a particular photopigment appears to exhibit little influence on the spectrum. It is in these spectral regions that another photopigment may be most optimally determined. At present too little data exist to evaluate the potential of this latter finding. It is possible that the three-band curvature algorithm given here is only indirectly responding to phycoerythrin. For example, if phycoerythrin is highly correlated to another pigment, say phycocyanin, the algorithm may actually be measuring the latter pigment. Thus the high correlation of the active and passive phycoerythrin measurements may be occurring via the covariability of another pigment.

The algorithm efforts described herein were initiated to identify algorithms which could recover planktonic chlorophyll accessory pigments from upwelled

spectral radiances. The ultimate objective is to develop passive techniques for detection and mapping of chlorophyll and accessory pigments from satellite platforms. This should in turn greatly assist in development and production of global plankton species maps. In the very long term it is hoped that spaceborne lidar techniques can complement passive systems much as they presently do on airborne platforms.[7,8]

The authors wish to extend their personal thanks to the many persons involved with the scientific field experiments, the AOL project, and aircraft operations. We are particularly indebted to the Instrument Electro-Optics Branch for the loan of the frequency-doubled Nd:YAG laser used to obtain the active data. We also thank the Ocean Processes Branch of NASA Headquarters for continued support and encouragement. AOL system calibration assistance by the Sensor Evaluation Branch of GSFC and by Warren Hovis and Jack Knoll of the NOAA National Environment Satellite Data and Information Service is gratefully acknowledged. Finally, the authors thank Gary Grew for participation in the field experiments and for the MOCS data.

References

1. W. Strumm and J. Morgan, *Aquatic Chemistry* (Wiley, New York, 1981).
2. H. R. Gordon and A. Y. Morel, "Remote Assessment of Ocean Color for Interpretation of Satellite Visible Imagery, A Review," in *Lecture Notes on Coastal and Estuarine Studies* (Springer-Verlag, New York, 1983).
3. F. E. Hoge and R. N. Swift, "Application of the NASA Airborne Oceanographic Lidar to the Mapping of Chlorophyll and Other Organic Pigments," in *Chesapeake Bay Plume Study Superflux 1980*, NASA Conf. Publ. 2188, 349 (1981).
4. F. E. Hoge and R. N. Swift, "Airborne Simultaneous Spectroscopic Detection of Laser-Induced Water Raman Backscatter and Fluorescence from Chlorophyll *a* and Other Naturally Occurring Pigments," Appl. Opt. **20**, 3197 (1981).
5. F. E. Hoge and R. N. Swift, "Airborne Dual Laser Excitation and Mapping of Phytoplankton Photopigments in a Gulf Stream Warm Core Ring," Appl. Opt. **22**, 2272 (1983).
6. F. E. Hoge and R. N. Swift, "Airborne Mapping of Laser-Induced Fluorescence of Chlorophyll *a* and Phycoerythrin in a Gulf Stream Warm Core Ring," paper 18, in *Mapping Strategies in Chemical Oceanography*, A. Zirino, Ed. (American Chemical Society, Washington, DC, 1985), pp. 353–372.
7. F. E. Hoge, R. E. Berry, and R. N. Swift, "Active-Passive Airborne Ocean Color Measurement. 1: Instrumentation," Appl. Opt. **25**, 39 (1986).
8. F. E. Hoge, R. N. Swift, and J. K. Yungel, "Active-Passive Airborne Ocean Color Measurements. 2: Applications," Appl. Opt. **25**, 48 (1986).
9. M. Bristow, D. Nielsen, D. Bundy, and F. Furtek, "Use of Water Raman Emission to Correct Airborne Laser Fluorosensor Data for Effects of Water Optical Attenuation," Appl. Opt. **20**, 2889 (1981).
10. R. C. Smith, U. California, Santa Barbara; personal communication.
11. D. A. Kiefer, "Chlorophyll *a* Fluorescence in Marine Centric Diatoms: Responses of Chloroplasts to Light and Nutrient Stress," Mar. Biol. **23**, 39 (1973).
12. R. H. Wiens and H. H. Zwick, "Trace Gas Detection by Correlation Spectroscopy," in *Infrared, Correlation and Fourier Transform Spectroscopy*, J. S. Mattson, H. B. Mark, Jr., and H. C. MacDonald, Jr., Eds. (Marcel Dekker, New York, 1977), Chap. 3, pp. 119–190.
13. R. A. O'Neil, L. Buja-Bijunas, and D. M. Rayner, "Field Performance of a Laser Fluorosensor for the Detection of Oil Spills," Appl. Opt. **19**, 863 (1980).
14. P. G. Hasell, Jr., L. M. Peterson, F. J. Thomson, E. A. Work, and F. J. Kriegler, "Active and Passive Multispectral Scanner for Earth Resources Applications," Final Report under NASA Control NAS9-14594 to Environmental Research Institute of Michigan, ERIM Report 115800-49-F (June 1977).
15. D. R. Lyzenga, "Remote Bathymetry Using Active-Passive Techniques," in *IEEE Digest of the International Geoscience and Remote Sensing Symposium, Vol. 2* (June 1981), pp. 775–786.
16. G. W. Grew and L. S. Mayo, "Ocean Color Algorithm for Remote Sensing of Chlorophyll," NASA Tech. Paper 2164 (Langley Research Center, Hampton, VA, 1983).
17. G. W. Grew, "Real-Time Test of MOCS Algorithm During Superflux 1980," in *Chesapeake Bay Plume Study Superflux 1980*, NASA Conf. Publ. 2188 (1981).
18. J. W. Campbell and W. E. Esaias, "Basis for Spectral Curvature Algorithms in Remote Sensing of Chlorophyll," Appl. Opt. **22**, 1084 (1983).
19. S. Lin, G. A. Borstad, and J. F. R. Gower, "Remote Sensing of Chlorophyll in the Red Spectral Region," in *Remote Sensing of Shelf Sea Hydrodynamics*, J. C. J. Nihoul, Ed. (Elsevier, Amsterdam, 1984), pp. 317–336.
20. R. A. Neville and J. F. R. Gower, "Passive Remote Sensing of Phytoplankton via Chlorophyll *a* Fluorescence," J. Geophys. Res. **82**, 3487 (1977).
21. J. F. R. Gower, "Observations of *in situ* Fluorescence of Chlorophyll in Saanich Inlet," Boundary Layer Meteorol. **18**, 235 (1980).
22. H. R. Gordon, D. K. Clark, J. W. Brown, O. B. Brown, R. H. Evans, and W. W. Broenkow, "Phytoplankton Pigment Concentration in the Middle Atlantic Bight: Comparison of Ship Determinations and CZCS Estimates," Appl. Opt. **22**, 20 (1983).
23. L. R. Poole and W. E. Esaias, "Water Raman Normalization of Airborne Laser Fluorosensor Measurements: A Computer Study," Appl. Opt. **21**, 3756 (1982).
24. A. F. Bunkin, D. V. Vlaso, D. M. Mirkamilov, and V. F. Sobodyanin, "Aerial Laser Sounding of the Turbidity Profile and Mapping of the Distribution of Phytoplankton," Dokl. Akad. Nauk SSSR **279**, 335 (1984). [NASA Tech. Memo. 77851 (1985)].
25. R. C. Smith and K. S. Baker, "Optical Classification of Natural Waters," Limnol. Oceanogr. **23**, 260 (1978).
26. J. J. Walsh, U. South Florida; private communication (manuscript in preparation).
27. C. M. Moreth and C. S. Yentsch, "A Sensitive Method for the Determination of Open Ocean Phytoplankton Phycoerythrin Pigments by Fluorescence," Limnol. Oceanogr. **15**, 313 (1970).
28. D. E. Stewart, "A Method for the Extraction and Quantitation of Phycoerythrin from Algae," NASA Contractor Report 165995 by Bionetics Corp. under contract NAS1-16978, Hampton, VA.
29. M. P. F. Bristow, D. H. Bundy, C. M. Edmonds, P. E. Ponte, E. E. Frey, and L. F. Small, "Airborne Laser Fluorosensor Survey of the Columbia and Snake Rivers: Simultaneous Measurements of Chlorophyll, Dissolved Organics and Optical Attenuation," Int. J. Remote Sensing **6**, 1707 (1985).
30. S. W. Jeffrey, "Algal Pigment Systems," in *Primary Productivity in the Sea*, P. G. Falkowski, Ed. (Plenum, New York, 1980).
31. R. J. Exton, W. M. Houghton, W. Esaias, R. C. Harriss, F. H. Farmer, and H. H. White, "Laboratory Analysis of Techniques for Remote Sensing of Estuarine Parameters Using Laser Excitation," Appl. Opt. **22**, 54 (1983).